1

Calibration of DEM Parameters

Corné Coetzee[1] and André Katterfeld[2]

[1] Stellenbosch University, Department of Mechanical and Mechatronic Engineering, Granular Materials Research Group, Joubert Street, Stellenbosch, 7600, South Africa
[2] Otto von Guericke University Magdeburg, Chair of Material Handling, Institute of Logistics and Material Handling Systems, Universitätsplatz 2, 39106 Magdeburg, Germany

Abbreviations and Acronyms

AoR	Angle of Repose
BCA	Bulk Calibration Approach
CFD	Computational Fluid Dynamics
CoR	Coefficient of Restitution
CPU	Central Processing Unit
DEM	Discrete Element Method/Discrete Element Modelling
DMA	Direct Measurement Approach
FEM	Finite Element Method
GPR	Gaussian Process Regression
GPU	Graphical Processing Unit
GSMC	Generalised Surrogate Modelling-based Calibration
MPM	Material Point Method
PSD	Particle Size Distribution
UCT	Uniaxial Compression Test

1.1 Introduction

Mesh-based simulation techniques in continuum mechanics, such as the Finite Element Method (FEM) or Computational Fluid Dynamics (CFD), require the body or volume of interest to be discretised by a mesh. The mesh closely represents the real object with small differences or idealisations, mostly directly proportional to the size of the mesh. These approaches show the convergence of the results with mesh refinement. However, Lagrangian approaches, such as FEM, suffer from severe mesh distortion when the body experiences large deformation. In these cases, the

Simulations in Bulk Solids Handling: Applications of DEM and other Methods, First Edition.
Edited by Don McGlinchey.

solution can become unstable, and the results inaccurate. The so-called meshless continuum-based methods such as the Material Point Method (MPM) are capable of modelling larger deformation [1]. However, these methods still assume a continuum body and might still rely on a non-deforming mesh. As a result, these methods cannot model the discrete nature of granular materials such as mixing and segregation or single particles separated from the bulk of the material in a screening process, for example.

The Discrete Element Method (DEM) was developed by Cundall and Strack [2] in the 1970s in order to solve problems associated with rock mechanics. The potential of DEM was quickly recognised for research purposes in a number of areas such as physics, nanotechnology, chemical engineering, and materials handling. DEM is completely meshfree (or meshless) and can easily model the large deformation typically associated with the handling and flow of bulk granular materials (particulate matter). DEM can also model the discrete nature of the individual particles, during screening for example.

To use DEM to analyse the behaviour of bulk materials, for example, in conveyor systems, during transportation and storage and flow through processing equipment, an accurate simulation model should be generated. A DEM model should define the geometric properties of the particles, such as the size and shape distributions, as well as the geometry of any structure or equipment. The interaction or contact properties (particle–particle and particle–wall) also need to be defined, which is a major component of the modelling process. As in all the numerical simulation methods, the experience (know-how) and sometimes the art applied by the user are critical to define and create a model capable of producing the most accurate simulation results in the shortest possible time frame.

In a DEM model, the discretisation of the bulk material is directly related to the size of the considered particles, which have a significant influence on the behaviour of the modelled material. DEM is also computationally intensive, and for this reason, most practical models are simplified in terms of particle size, shape, and contact properties. This idealisation is the reason why established bulk material properties (e.g. the angle of internal friction and the angle of repose [AoR]) cannot be directly used as input parameters. Hence, it is necessary to reverse engineer the parameters by comparing the modelled bulk behaviour to that observed in the experimental tests. This procedure is called the ‘calibration of DEM parameters’ and is the key to produce realistic simulation results.

1.2 Basic DEM Theory

A typical DEM model consists of particles and walls. The particles can make contact with one another and with walls, but wall–wall contact is usually undefined. The particles represent the granular material and can in theory take on any shape and size. However, in practice, spherical and multi-sphere particles are the most commonly used. Walls are used to define all the structures with which the particles can interact, such as the walls of equipment and machines. Contact models are used to calculate the contact forces and moments based on the contact kinematics.

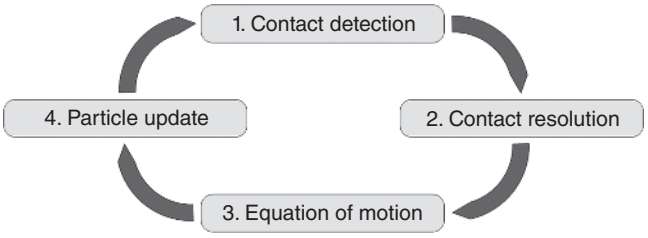

Figure 1.1 DEM computation cycle.

1.2.1 The Calculation Cycle

A DEM calculation cycle consists of four steps as illustrated in Figure 1.1, namely (1) contact detection, (2) contact resolution, (3) solving the equation of motion, and (4) updating of the particle velocity and position.

The contacting pieces (particles and walls) are allowed to overlap, and in the first step of the computation cycle, all particle–particle and particle–wall contacts are identified. The overlap is assumed to be relatively small compared to the particle size. Although contact detection happens automatically, without any user intervention, the particle shape selected by the user has a significant effect on the efficiency of this step. Spherical particles are computationally the best, followed by multi-sphere particles and more complex shape representations such as super-quadrics and polyhedra.

In the second step, the force and moment vectors are calculated at each contact, based on one of a number of available contact models selected by the user. The contact force and moment are dependent on the relative contact displacement or overlap (elastic force), velocity (viscous force) and the contact parameter values specified by the user.

In the third step, the resultant force and moment acting on each particle are calculated. This includes the forces, $\mathbf{F}_c$, and moments, $\mathbf{M}_c$, due to the contacts and the body force due to gravity $\mathbf{F}_g$. Based on the particle's mass, m, and moment of inertia, I_g, the translational acceleration, $\ddot{\mathbf{x}}$, and the rotational acceleration, $\ddot{\boldsymbol{\theta}}$, can be calculated using the equations of motion,

$$\ddot{\mathbf{x}} = \frac{\mathbf{F}_c + \mathbf{F}_g}{m} \tag{1.1}$$

$$\ddot{\boldsymbol{\theta}} = \frac{\mathbf{M}_c}{I_g} \tag{1.2}$$

In the fourth and last step, the particle velocity (translational $\mathbf{v} = \dot{\mathbf{x}}$ and rotational $\boldsymbol{\omega} = \dot{\boldsymbol{\theta}}$) is first updated using an explicit time integration scheme,

$$\mathbf{v}^{t+\Delta t} = \mathbf{v}^t + \ddot{\mathbf{x}}\Delta t \tag{1.3}$$

$$\boldsymbol{\omega}^{t+\Delta t} = \boldsymbol{\omega}^t + \ddot{\boldsymbol{\theta}}\Delta t \tag{1.4}$$

where Δt is the timestep. This is followed by the particle's position and orientation update,

$$\mathbf{x}^{t+\Delta t} = \mathbf{x}^t + \mathbf{v}^{t+\Delta t}\Delta t \tag{1.5}$$

$$\boldsymbol{\theta}^{t+\Delta t} = \boldsymbol{\theta}^t + \boldsymbol{\omega}^{t+\Delta t}\Delta t \tag{1.6}$$

The explicit time integration scheme is conditionally stable and requires a timestep smaller than the critical timestep. Using the analogy of a single degree-of-freedom mass-spring system, it can be shown that the stable timestep is proportional to the particle mass and inversely proportional to the effective contact stiffness. For slight variations in the explicit time integration scheme and the calculation of the timestep, see O'Sullivan [3] for example.

This step concludes the basic time cycling sequence, after which the time is incremented, followed by a new contact detection step.

1.2.2 Contact Models

A contact model defined at each contact describes the force–displacement relation. There are a number of contact models from which the user can select. Figure 1.2 shows the basic elements of a contact model, namely springs, dashpots, frictional sliders, and tension elements. A combination of these elements act in each of the normal and shear (tangential) directions.

The spring elements define the elastic force component and can have linear behaviour (as in the linear model) or non-linear behaviour (as in the Hertz–Mindlin model). The viscous dashpots dissipate energy, and the frictional slider allows for Coulomb-like frictional behaviour in the shear direction. For the modelling of spheres, rolling resistance models are very important; however, they are not visualised in Figure 1.2. Cohesive behaviour can be modelled by allowing tensile forces in the normal direction. The details of the different contact models are not presented here, and the interested reader should consult other sources such as O'Sullivan [3] and Thornton [4].

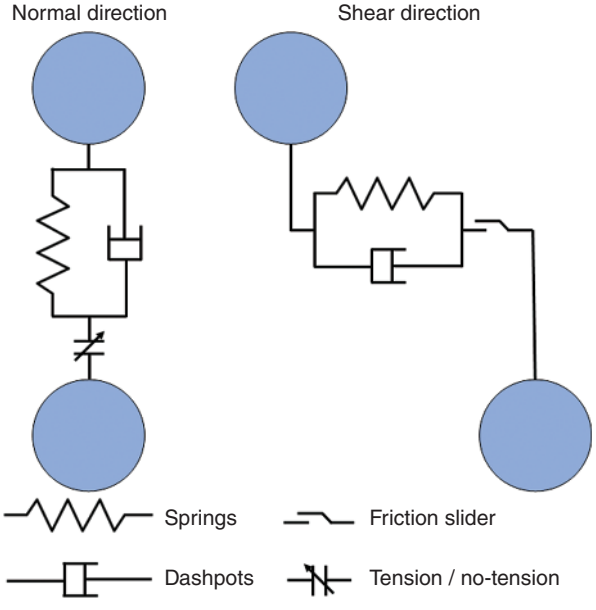

Figure 1.2 Typical elements of a contact model.

At each timestep, the relative motion between two contacting pieces is used, in combination with the elements defined above, to update the contact force components. The user should specify the parameter values for the spring stiffness, for example the damping (dashpot) constants and the coefficient of friction. Obtaining a set of parameter values so that the modelled bulk behaviour of the material is an accurate representation of a physical material is the main focus of the calibration process.

1.3 DEM Application and Calibration Philosophies

In general, the application of DEM can be classified in two groups:

- **Group 1** focuses on improving our general understanding of the physics (e.g. rheology, constitutive behaviour) of granular materials through applied research [5, 6]. For this purpose, idealised ('artificial' or manufactured) bulk materials such as glass beads with a very well-defined particle size distribution (PSD) (mono-disperse or bi-disperse) and (close to) homogeneous properties are used. Often the particle behaviour is investigated in small-scale laboratory tests with a relatively small number of particles involved. The DEM model replicates the real application with a scale of 1 : 1, even if it requires a very large computational effort and duration of time.
- **Group 2** focuses on the modelling of 'natural' bulk materials in industrial applications. The materials range from powders to rocks and require an idealisation of the DEM models in terms of particle shape, size distribution, and stiffness.

In the first group of applications, it is possible to use tests to determine the particle or contact micro-properties and directly use them as DEM input parameters. This approach or philosophy for DEM parameter selection was labelled the 'Direct Measurement Approach' (DMA) by Coetzee [7].

In the second group of applications, the DMA can at most be partly used, since there are a number of simplifications required. For these applications, the macroscopic (bulk) material behaviour needs to be replicated by an idealised DEM model. Hence, the microscopic DEM parameters are to be chosen in such a way that the macroscopic behaviour of the material in the simulation is the same as that in reality. According to Coetzee [7], this approach is called the 'Bulk Calibration Approach' (BCA) since the process of finding the DEM parameters is an iterative process that involves a series of simulations which replicate at least one experiment. This approach truly earns the name 'calibration', and in the sections to follow, the term calibration refers to BCA, unless stated otherwise.

Although the process of parameter selection using the BCA is essential to produce simulations with realistic results, there are only a few works which try to define a systematic approach for the BCA. Especially in the industrial sector, many calibration approaches do not earn the name 'calibration'. The selection of DEM parameters based on a non-systematic parameter selection ('guessing of parameters') may lead

to wrong DEM results and invalid conclusions. This may also be the case when DEM parameters are 'tuned' based on simulations of the final application, where the parameters are non-systematically varied until the flow results look like what is expected.

Furthermore, the kind of applications being modelled can also influence the calibration experiments and DEM parameters to be used (the selection of appropriate contact models, for example). Here the focus is on bulk storage and handling applications where the consolidation pressure is relatively low (less than 10 kPa), and the material is either static (storage in a bin or moving with a conveyor belt, for example) or dynamic and flowing (out of a bin or through a transfer chute, for example). When the material is under higher consolidation pressure, aspects such as plasticity might become important, which is not addressed in this work.

To ensure that the DEM simulation results can be trusted, the user must have a basic understanding of the physical bulk properties and the most important DEM parameters. This is addressed in the next sections, followed by a detailed discussion of the calibration process.

1.4 Physical Bulk Properties

The properties that are important for bulk handling applications are discussed. It is important to consider all these bulk properties during the calibration process.

1.4.1 Bulk Density and Porosity

Bulk density is needed to accurately model the body forces due to gravity and hence the consolidation pressure (even if relatively low) experienced by a bed of material. Bulk density is also important to accurately model the forces exerted by the material on structures or equipment walls. When the material flow rates are considered (modelling the conveying of material, for example), it is important to accurately model not only the mass flow rate but also the volume flow rate. The cross-sectional area of a transfer chute, for example, should be sufficient to handle the volume flow rate, which is related to the mass flow rate by the bulk density.

1.4.2 Bulk Friction

In this chapter, the term 'bulk friction' is used to define and characterise the bulk property related to the material's resistance to shear flow. Physically, the bulk friction is influenced by the PSD, particle shape, and inter-particle sliding friction. The particle shape leads to mechanical interlocking, which results in shear resistance even under zero normal load. The Coulomb-type sliding friction at contacts has a significant effect on the bulk friction. On the bulk level, the material can be considered a continuum and described by the Mohr–Coulomb constitutive model, defining a bulk cohesion and internal friction angle (yield locus) which can be measured in a direct shear test, for example.

1.4.3 Dissipation of Energy

In non-cohesive bulk materials, energy is dissipated in the form of contact friction, inelastic deformation of the particles and walls, particle breakage (fracture energy), and other losses such as wind resistance. Losses due to wind resistance and particle breakage are usually ignored, unless multiphase flow (coupled CFD–DEM modelling) or particle breakage is specifically analysed. Contact friction is responsible for the majority of the energy dissipated and should be accurately accounted for in all DEM models.

Additional contact damping (usually viscous damping) is required to reach a state of static equilibrium, when particles are dropped from a height into a bin, for example. However, appropriate levels of damping are also required for dynamic processes to keep the energy levels realistic and to avoid excessive particle motion.

1.4.4 Bulk Stiffness

When a bed of material is compressed, the relation between the applied force and the displacement (change in bed height) defines bulk stiffness. The stiffness can be measured under confined and unconfined conditions (these two approaches will result in different stiffness values).

Even if the inter-particle contact stiffness is linear, bulk stiffness is not necessarily linear. The non-linearity in bulk stiffness is caused by re-organisation of the position of the particles and contacts in the packing – increasing the number of contacts under increasing load. Due to this phenomenon, initial cyclic loading-and-unloading compression of a loosely packed particle bed results in hysteretic behaviour, where the unloading curve shows increased stiffness as compared to the loading curve.

1.4.5 Bulk Cohesion and Adhesion

In general, the term ‘cohesion’ refers to the attractive force between two similar materials, and the term ‘adhesion’ to the attractive force between two dissimilar materials. Here, however, the two terms are used interchangeably. The bulk cohesive behaviour is due to cohesive forces acting at the contact level (particle–particle and particle–wall), where it is mainly caused by one of two mechanisms: liquid-bridges or Van der Waals forces.

When moisture or liquid (mostly water in the applications considered here) is introduced, a thin liquid film forms on the outer surface of the particles and walls. When a new contact forms, a liquid bridge is formed, resulting in a tensile force due to the capillary effect and liquid surface tension (see Mitarai and Nori [8], for example). The van der Waals force, on the other hand, acts between two macroscopic bodies due to intermolecular cohesion forces, and the effects are significant only for very small particles such as powders ($<100\,\mu m$, [9]). Independent of the cohesion mechanism at the contact level, an increase in contact cohesion results in an increase in bulk cohesion. Here, the term bulk cohesion refers to the bulk material’s resistance to shear flow under zero normal load.

1.5 DEM Parameters and Their Relation to Bulk Properties

The DEM contact parameters discussed in this section are generic and applicable to all non-cohesive contact models, including linear and non-linear models. These are the parameters that should in general be considered and calibrated to ensure accurate modelling of the applications considered in this chapter. Although the implementation of these generic parameters is dependent on the specific contact model (and even the software) used, the relation with bulk properties as described here will remain valid.

The DEM parameters and bulk properties considered are listed in Table 1.1. The first three parameters (particle shape, size, and density) are related to the particles, while the other parameters are all related to the contacts (particle–particle and particle–wall). The relation between each parameter and bulk property (as discussed in Section 1.2) is indicated as either 'strong', 'weak', or 'negligible' (insignificant), and the effect of the parameter on the computation time is also indicated. These relations are further discussed below, and typical calibration experiments for each bulk property are listed at the bottom of the table.

1.5.1 Particle Shape

Discrete elements are used in DEM to represent the particles. In general, these elements are referred to as particles, and pioneering DEM codes [2] were used for circular (in 2D) and spherical (in 3D) particles due to the associated computational efficiency in contact detection and overlap calculation. However, with advances in computing power, more complex non-spherical shapes were introduced using different techniques as discussed below.

The particle shape will influence all the other model parameters that need to be calibrated and should be the first parameter to be decided by the modeller. If, at any later stage, the shape is changed or even slightly modified, all the parameter values should be re-calibrated. When the physical particles are non-spherical (which is the case in most industry and practical applications), the user has the option to make use of spherical particles and include rolling resistance or to make use of one (or more) of the available non-spherical shape models (with or without rolling resistance).

1.5.1.1 Non-spherical Particles

Any number of spheres can be merged to form a single particle, often referred to as 'multi-sphere particles', 'clumps', 'clusters', or 'glued particles'. The constituent spheres can overlap, and their relative position within the particle remains fixed, thus creating a rigid particle. Multi-sphere particles still allow for efficient contact detection and overlap calculation. However, these particles still have some limitations, and sharp edges or blocky particles cannot be easily created. Multi-sphere particles also have 'bumpy' surfaces, which might introduce higher levels of interlocking and tend to have more contacts with other particles and walls.

Table 1.1 Relation between DEM parameters and non-cohesive bulk properties.

	Bulk material properties				
DEM parameters	**Bulk density and porosity including changes due to flow (dilatancy)**	**Bulk friction/shear/ interlocking/flow behaviour**	**Dissipation of energy (damping)**	**Bulk stiffness**	**DEM model computation time**
Particle shape	**Weak** Influences the packing porosity, and hence the bulk density for a given particle (solid) density.	**Strong** The more non-spherical the shape, the higher is the interlocking effect, and thus, the higher the bulk friction.	**Negligible**	**Negligible**	**Strong** Spherical particles are the most efficient. The more complex the shape, the longer a defined simulation takes to complete.
Particle size distribution (PSD)	**Weak** Influences the packing porosity, and hence the bulk density. The wider the PSD, the lower is the porosity and the higher is the bulk density.	**Weak** The wider the PSD, the lower is the porosity and the higher is the particle interlocking, thereby increasing the resistance to shear.	**Negligible**	**Negligible**	**Strong** A reduction in the number of particles, logarithmically reduces the computation time.
Particle density	**Strong** The relation between particle density and bulk density is very close to linear for a given porosity (i.e. particle shape and size distribution).	**Negligible**	**Negligible**	**Negligible**	**Strong** The time step increases in size with an increase in density, thus reducing the total simulation time.

(Continued)

Table 1.1 (Continued)

	Bulk material properties				
DEM parameters	**Bulk density and porosity including changes due to flow (dilatancy)**	**Bulk friction/shear/ interlocking/flow behaviour**	**Dissipation of energy (damping)**	**Bulk stiffness**	**DEM model Computation time**
Contact damping/ coefficient of restitution	**Negligible**	**Negligible**	**Strong** Contact damping (together with sliding and rolling friction) is one of the major mechanisms for the dissipation of energy.	**Negligible**	**Negligible**
Contact stiffness	**Negligible** Using realistic values, the contact stiffness has a negligible effect on the bulk density. Very low values will increase the contact overlap and the bulk density. However, if this is the case, the stiffness is probably too low for modelling the typical materials considered here.	**Negligible** The contact stiffness has an effect on the bulk friction only for unrealistically low stiffness values which should be avoided [10].	**Negligible** If the user specifies either the non-dimensional critical damping ratio or coefficient of restitution, the effect is negligible since the code will calculate the damping constant based on this value in combination with the stiffness.	**Strong** The contact stiffness has a strong relation to the bulk stiffness. With an increase in the contact stiffness, the bulk stiffness increases.	**Strong** The contact stiffness highly influences the time step: the higher the stiffness, the smaller is the time step. Due to this effect, most DEM simulations make use of a reduced stiffness.

Contact coefficient of sliding friction: particle–particle	**Weak** Higher friction values lead to less dense packings (slightly higher porosity).	**Strong** The sliding friction is one of the major parameters influencing the bulk shear behaviour. An increase in the friction increases the bulk friction asymptotically: for lower friction coefficients, the bulk friction is more sensitive than for higher friction coefficients (typically 0.7 and higher).	**Strong** The sliding friction is one of the major mechanisms for energy dissipation.	**Negligible**	**Negligible**
Contact coefficient of sliding friction: particle–wall	**Negligible**	**Strong** The sliding friction is one of the major parameters influencing the bulk shear behaviour against a structure or wall. For example the flow down a chute or out of a bin.	**Strong** The sliding friction is one of the major mechanisms for energy dissipation, although quantitatively less than particle–particle friction.	**Negligible**	**Negligible**

(Continued)

Table 1.1 (Continued)

	Bulk material properties				
DEM parameters	**Bulk density and porosity including changes due to flow (dilatancy)**	**Bulk friction/shear/ interlocking/flow behaviour**	**Dissipation of energy (damping)**	**Bulk stiffness**	**DEM model Computation time**
Contact coefficient of rolling friction (particles and walls)	**Negligible**	**Strong** The rolling friction, in combination with the sliding friction, has a strong influence on the bulk friction (shear) behaviour.	**Negligible**	**Negligible**	**Negligible**
Experiments that are sensitive to the specific bulk material property	Bulk density/porosity: Filled container Dilatancy: Direct shear test	Angle of repose Discharge test Draw down test Direct shear test	Drop test Pendulum test Uniaxial compression	Uniaxial compression	—

Non-spherical particle shapes can also be modelled using mathematical descriptions such as superquadrics, polyhedra, and faceted particles. The advantages of this technique include the modelling of complex shapes more accurately, including blocky particles and sharp edges; however, it comes with a decrease in computational efficiency.

In general, when non-spherical particles are used, rolling resistance (friction) can be omitted if the selected shape can be accurately calibrated using only sliding friction [11].

1.5.1.2 Spherical Particles

The contact model for spherical particles should include rolling resistance to realistically model the rotational behaviour of physical non-spherical particles. Various authors (e.g. [11–14]) have shown that rolling resistance can accurately account for the particle shape in terms of bulk behaviour. Wensrich et al. [15] showed that spherical particles with rolling friction can accurately model the behaviour of non-spherical particles in both static and dynamic flow conditions with the dilational nature also captured to a reasonable degree. Several rolling resistance models are available as summarised by Ai et al. [16], and according to Wensrich and Katterfeld [17], Type C is the preferred and most stable model.

1.5.1.3 Shape Selection

If the bulk material has a relatively homogeneous particle size and shape, it is suggested to make use of spherical particles with rolling resistance. This is applicable to materials such as sand, crushed gravel, mineral ore, and agricultural grains and seeds. Also, when the material flow is relatively homogeneous, i.e. the material flows in a stream with little variation in particle velocity, the effect of particle shape becomes less significant, and a simple and efficient shape can be selected. In these cases, if non-spherical particles are used, it is proposed to use simple multi-sphere particles comprising three spheres in a pyramid shape [18, 19], where rolling resistance can be ignored.

In applications where the material is non-homogeneous in particle shape and size and where the particles are relatively large in comparison to the model boundaries (interacting with structures, equipment, and machine parts), the particle shape becomes more important. Also, if mixing, screening and sieving, or mechanical arching and bridging are investigated, accurate shape models should be considered [20]. The modelling of materials such as biomaterials might also require more accurate shape modelling if the particles are far from spherical, for example, wood chips and fibres [21, 22].

1.5.2 Particle Size Distribution and Scale

The PSD and scale (size) of calibration experiments are closely related. The PSD of the physical material being modelled can be measured using sorting sieves or screens. Alternative methods include photo analysis and laser diffraction

techniques. However, the modeller should decide how the PSD of the physical material will be modelled. Due to computational constraints, the maximum number of particles that can be modelled within a reasonable time frame is limited, depending on the available software and hardware (Central Processing Unit [CPU] versus Graphical Processing Unit [GPU], for example). In most industrial-scale applications the number of particles can easily be in billions to trillions [23], which cannot be modelled, regardless of the available hardware. In these cases, the number of particles should be reduced by scaling the PSD.

There are several approaches available for this, as described by Roessler and Katterfeld [24] and the references therein, namely exact scaling, coarse graining, scalping, and combined scaling. Mohajeri et al. [25] developed a hybrid scaling technique where the geometry and the particles are scaled in a stepwise manner. This technique requires more simulation runs, but it can be used for the calibration and validation of upscaled particles even if the available experimental setup is too small to accommodate the final upscaled particles and if the experiment is scale-dependent.

The final selection of the modelled PSD will depend on the physical PSD, the application being modelled, available calibration equipment, and the available computational power. There are no general rules and guidelines that apply to all possible cases. The PSD used in the calibration step should be identical to the PSD used in modelling the (full-scale) final application. Similar to the particle shape, once a PSD is calibrated, it cannot be modified, unless the calibration steps are repeated. As a general rule, the particle size should be selected so that there are at least 10–20 particles across all dimensions of the geometry. The particle resolution should be high enough to render realistic and accurate results within a reasonable time frame. With larger (fewer) particles, the resolution is reduced, and boundary (wall) effects become significant. When the flow of the material through an orifice is modelled, the ratio of the orifice opening to particle size should be as large as computationally possible to avoid any choking effects.

1.5.3 Particle Density

Despite the idealised PSD and particle shape, the bulk density can still be accurately modelled by calibrating the particle (solid) density. The best approach is to follow the technique often used to experimentally measure the material's bulk density. A container with known volume is filled with modelled particles, and the total particle weight is determined and used to calculate the modelled bulk density. Iteratively changing the particle density, the modelled bulk density will converge to the measured value (allow for static equilibrium to be reached after each change in particle density).

This process is suitable for the relatively low consolidation pressures (less than 10 kPa) and non-cohesive to slightly cohesive materials as considered in this chapter. For higher consolidation pressures and cohesive materials, the density test should

be performed with different consolidation pressures or at least in the same range of pressures that the material will be subjected to in the final application.

1.5.4 Contact Damping

The dissipation of energy is accounted for by frictional contacts and by introducing viscous damping at the contacts. Viscous damping is modelled as a dashpot in parallel to the contact stiffness (spring). In general, depending on the specific software implementation, the level of damping can be specified in one of three ways:

1. Directly providing the damping coefficient in units of $\mathrm{Ns\,m^{-1}}$
2. Specifying the dimensionless critical damping ratio, ζ
3. Specifying the dimensionless coefficient of restitution (CoR)

1.5.5 Contact Stiffness

In DEM, the stiffness in the normal and tangential directions is used to calculate the contact forces. The formulation of the stiffness depends on the specific contact model used, and commonly used models include the Hertz–Mindlin (no-slip) model and the linear model.

In the linear contact model, the normal stiffness and tangential stiffness are independently specified in units of $\mathrm{N\,m^{-1}}$, i.e. linear spring elements. In the Hertz model, the particle's elastic properties are specified, either the Young's modulus or shear modulus, and Poisson's ratio. Based on these properties, the non-linear normal stiffness and tangential stiffness are calculated, which is a function of the overlap.

With the Hertz–Mindlin contact model, realistic bulk flow results can often be achieved using relatively low values for Young's modulus, starting at 1e7 Pa [24, 26, 27], and calibration is not necessary and often not performed. For the linear contact model, a lower-end contact stiffness is in the order of $\mathrm{1e4\,N\,m^{-1}}$. If forces or pressures have to be predicted, it must be determined how the reduction of the Young's Modulus will influence the simulation results, see for example, the detailed description by [27].

1.5.6 Particle–Particle Sliding Friction

The particle–particle coefficient of friction considered here cannot be measured directly due to their shape and size. But even if it could be measured, the shape and size are almost always simplified for computational efficiency. The whole calibration process compensates for these simplifications, and in the end, the combination of particle shape, size, sliding, and rolling friction has to produce realistic bulk flow behaviour. Thus, the final value used for the coefficient of sliding friction is not necessarily equal to that between two physical particles of the same material.

1.5.7 Particle–Wall Sliding Friction

The particle–wall sliding coefficient of friction can be directly measured in wall shear tests or inclined wall (plane) tests. In the applications considered here, the modelled bulk behaviour is usually less sensitive to the particle–wall friction than to the particle–particle friction.

1.5.8 Contact Rolling Friction

The rolling friction of non-spherical particles cannot be directly measured. Often different values are used for the rolling friction of particle–particle and particle–wall contacts. However, due to the fact that the rolling friction compensates primarily for the effect of the particle shape, the same value can be used for both. When spherical particles are used, rolling friction should be included, but when non-spherical particles are used, the inclusion of rolling friction will depend on the exact shape used [11].

1.6 Overview of Calibration Tests

The main objective of the calibration process is to compare the results from an experiment and a simulation, from which the DEM parameters are then derived, which will provide the most realistic and accurate results. Most calibration experiments need to consider the macroscopic (bulk) material behaviour, i.e. the behaviour of the interaction of a large number of particles (BCA). However, there are a small number of DEM parameters for which it is sufficient to investigate single particle/contact behaviour (DMA, e.g. a drop test to determine the CoR).

Standard tests for measuring bulk material properties include direct shear tests, using either translational (Jenike) or rotational (Schulze) shear testers. However, due to the complexity and the time duration of these tests, other non-standard tests were developed.

Katterfeld et al. [28] proposed in a White Paper that the calibration experiment should be chosen according to the real bulk material's flow mechanism in the final (industrial) application. If, for example, the final aim is to optimise the design of a transfer chute with a relatively fast flow regime and low to medium consolidation (typically $\ll 100$ kPa), the calibration experiment should consider the same flow regime. If compaction or comminution processes are analysed, a different set of calibration tests might be more appropriate.

Due to the very large variety of bulk solid handling applications, where DEM simulations may be of interest, it is not possible to describe each calibration experiment. The following calibration tests, each having advantages and disadvantages, can be used to study applications with fast flow regimes and low to medium consolidation as mentioned above. Coetzee [11] showed that the results of a proper calibration procedure can be reproduced by a different calibration procedure by using different experiments.

1.6.1 Basic Requirements for Calibration Tests

Due to the many possibilities, it is beneficial to define some practical evaluation criteria for the calibration tests. A typical test should:

- be simple and quick to undertake, both experimentally and numerically (simulation).
- Require only a small amount of bulk material.
- Provide a test result that can be easily measured or determined (experimentally and in the simulation).
- Be scale invariant. This means that the procedure should provide the same test results independent of the physical size of the test apparatus. The determination of an angle (such as the AoR for example) is typically invariant to the size of the particles and the test setup, as long as the flow mechanism which leads to the formation of the angle, is not significantly influenced by the size of the setup used [24].
- Produce consistent results. Due to the discrete (stochastic) nature of granular materials, two identical experiments will not necessarily provide identical results. Experiments should be repeated, and the results statistically analysed to obtain at least an average value and the standard deviation. Ideally, the experiment should produce consistent results, with a relatively small standard deviation.

All these tests do not necessarily result in the same AoR. This is mainly due to differences in the particle kinetic energy during the execution of the test, which influences the settling of the particles. Therefore, it is also important to simulate the exact same test and not to directly compare the AoR from one test apparatus to that of another.

All tests typically allow for an optical measurement of the AoR. The angle should be measured on a part of the slope where it is constant (approaching a straight line), and on several cross sections, so as to obtain an average value. Several image processing and measurement algorithms have been developed to ensure a consistent technique is applied and to eliminate human error in measuring the angle. A number of algorithms for experimental and simulation results can be found in Wensrich and Katterfeld [17], Tan et al. [30], Muller et al. [31], and Klanfar et al. [32].

1.6.2 Calibration Tests

Table 1.2 provides a brief summary and graphic representation of the most commonly used calibration tests from multiple studies. Since it is one of the most widely considered bulk material calibration tests (and parameter), the only test which should be explained in more detail is the AoR. To determine the AoR, several tests can be undertaken [31, 47]:

- Lifting cylinder test
- Funnel test (also called the hopper or drained test)
- Shear box (also called the ledge, slump, or rock box test)
- Cone test (also called the hourglass, sandglass, or trapdoor test)
- Rotating drum test (also called the dynamic AoR test)

Table 1.2 A summary and graphic representation of typical calibration tests.

Calibration test		Test properties: Scale effects	Test properties: Bulk measures for calibration	Test properties: Test effort, applicability	Comments and further references
Angle of repose tests	Lifting cylinder test 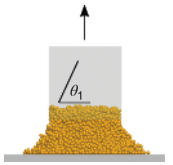	Scale invariant if the cylinder speed is adopted according to the scale.	The static AoR.	The test apparatus is very simple and easy to manufacture if not readily available (open-ended cylinder). The tests are simple and quick to execute (simulations and experimentally). Suitable for all PSD's if the cylinder diameter is selected to accommodate enough of the largest particles across its diameter.	The AoR is sensitive to the cylinder lifting speed. This effect can be significantly reduced if a relatively low speed is used. For further information see: Roessler and Katterfeld [29], Tan et al. [30], Muller et al. [31], Klanfar et al. [32], Qi et al. [33], Zhou et al. [34], Do et al. [35], Derakhshani et al. [36] and Elskamp et al. [37].
	Funnel test 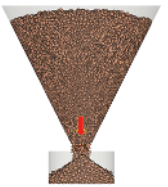	Scale variant due to the change in drop height.	The poured AoR.	The test apparatus is simple and easy to manufacture. The tests are simple and quick to execute (simulations and experimentally). Suitable for all sample and PSD sizes if the orifice is selected to accommodate enough of the largest particles across its diameter.	The AoR is sensitive to the drop height. The discharge time can be used as an additional calibration parameter (see the discharge test below). The formation of large-scale stockpiles can be seen as an industrial equivalent and a large-scale variant of this test. Due to the higher induced energy in the system, the AoR is usually lower than in the lifting cylinder test. Also, the difference in the AoR from different bulk materials is smaller than what it would be in the lifting cylinder test. Hence, if the measurement error is considered, the AoR measured in this test spans the same range for a variety of different materials. For further information see: Horabik et al. [38], Wang et al. [39], Fu et al. [40] and Chen et al. [41].

Shear box test 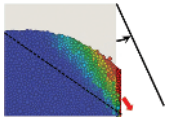	Scale invariant due to the rapid outflow.	The shear angle; the remaining mass.	The shear box is very simple and easy to manufacture, but must have transparent side walls for optical measurements. The tests are simple and quick to execute (simulations and experimentally). Suitable for all sample and PSD sizes.	The remaining mass in the shear box can be determined and used as an additional calibration parameter. For further information see: Derakhshani et al. [36], Do et al. [35], Roessler et al. [14], Lommen et al. [42], Pachon-Morales et al. [43], Mohajeri et al. [25].
Cone test 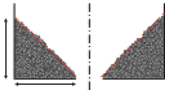	Scale variant due to the variable ratio between the orifice diameter and the particle size.	The shear angle (also called the drained AoR).	The test apparatus is simple and easy to manufacture. Typically, a transparent (glass or poly-glass) cylinder is used. The tests are simple and quick to execute (simulations and experimentally). Typically for small samples and fine-grained materials.	Due to the often cylindrical design it is very difficult to change the diameter of the orifice. The whole slope cannot be observed, only the height against the outer cylinder wall. Thus, a straight slope face is assumed in the calculation of the angle. For further information see: Do et al. [35], Derakhshani et al. [36], Horabik et al. [38] and Fu et al. [40].
Rotating drum test 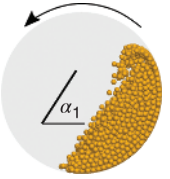	Scale variant.	The dynamic AoR.	The test apparatus is more complex to manufacture. It requires a rotating drum with a transparent side wall and an electrical drive and controller to ensure the drum rotates at constant speed. Compared to the experiments, the simulation model is easier to create. The tests are simple and quick to execute (simulations and experimentally). Typically for smaller samples and fine-grained material (powders).	Recommended to perform this test in the so-called rolling regime which is defined by the Froude number in the range $10^{-4} < Fr < 10^{-2}$ where $Fr = \omega^2 R/g$ with ω the rotation speed, R the drum radius and g the gravitational acceleration. Due to dynamic effects, the differences observed in the AoR from different bulk materials may be small. For further information see: Coetzee [11, 44], Elskamp et al. [37], Rong et al. [45].

(Continued)

Table 1.2 (Continued)

Calibration test	Test properties: Scale effects	Test properties: Bulk measures for calibration	Test effort, applicability	Comments and further references
Discharge test 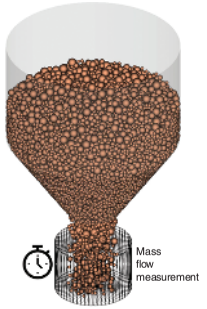	Scale variant due to the variable ratio between the opening and particle size.	The discharge time (duration); the general flow field if coloured particles and a transparent bin are used.	The test apparatus is simple and easy to manufacture. Almost any bin size and shape can be used. The tests are simple and quick to execute (simulations and experimentally). Suitable for all sample and PSD sizes if the opening diameter is selected to accommodate enough of the largest particles.	Stopwatch measurements are inaccurate due to the trickling down of material, and it is often hard to determine the precise moment when the bin is fully emptied. For further information see: Balevicius et al. [46], Derakhshani et al. [36], Hlosta et al. [47], Coetzee and Nel [48], Coetzee [18].
Draw down test 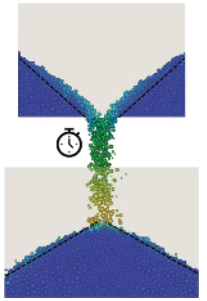	Scale variant.	The shear angle (upper box); the dynamic (poured) AoR (lower box); mass flow rate and/or remaining mass.	The test apparatus is very simple and easy to manufacture, but must have transparent side walls. The tests are simple and quick to execute (simulations and experimentally). Suitable for all small to medium sample and PSD sizes.	This test combines a number of other calibration tests into one: funnel test, shear box test, cone test and the discharge test. Rectangular design for easy change of discharge opening. Different opening settings allow for the studying of arching of cohesive materials. For further information see: Roessler et al. [14], Coetzee [11], Grima and Wypych [49], Derakhshani et al. [36], Do et al. [35], Zhou et al. [50].

Inclined wall friction test 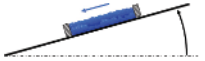	Scale invariant.	Direct measurement of the static friction angle; Measure the sliding or rolling speed to estimate the coefficient of dynamic friction and rolling friction, respectively.	The test setup is more complex to manufacture, if a manual process is not to be followed. The angle of the wall needs to be adjusted using a very slow and smooth action. For this purpose a dedicated motor- or mechanical drive is needed. The tests are simple and quick to execute. Suitable for all particle sizes. Rolling friction can only be estimated for (close to) spherical particle shapes.	Direct measurement of parameter values; hence, no need to replicate the test in a DEM simulation (DMA). For further information see: Barrios et al. [51], Wang et al. [39], Hlosta et al. [47], Agarwal et al. [52].
Direct shear tests 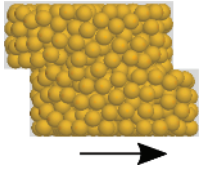	Scale variant.	Angle of internal friction; cohesion (apparent cohesion for non-cohesive materials); dilatant behaviour; material-wall friction angle.	The test apparatus is complex and should be carefully manufactured or, preferably, a commercial unit should be used. Tests are cumbersome to execute and require multiple steps (simulations and experimentally). Limited maximum particle size dependent on the available test cells (experiment). For a given maximum particle size, all PSDs can be accommodated.	To obtain a full yield locus, a series of tests are required which can take long to complete (simulations and experimentally). For detailed procedures, refer to the various standards, such as ASTM D3080/D3080M [53] and ISO 17892-10:2018 [54] for the translational Jenike shear tester, and ASTM D6773-16 [55] for the Schulze ring shear tester (rotational). These standard test procedures require several steps such as pre-shear and shear, especially for cohesive materials. For further information see: Coetzee [11, 18], Mohajeri et al. [25, 57], Simons et al. [56], Bian et al. [58] and Falke et al. [59], Grima and Wypych [60].

(Continued)

Table 1.2 (Continued)

Calibration test	Test properties: Scale effects	Test properties: Bulk measures for calibration	Test effort, applicability	Comments and further references
Confined uniaxial compression test 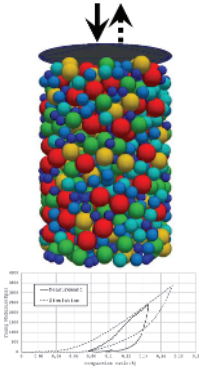	Scale invariant if the container is sufficiently large to accommodate enough particles per cross section.	Bulk stiffness.	Although the cylindrical container is simple and easy to manufacture, the test requires a universal tensile/compression or similar test machine. The simulation is easy to set up. The tests are simple and quick to execute. Suitable for all sample and PSD sizes, by selecting an appropriate container size.	Note that this test should not be confused with the uniaxial compression test [UCT] often used to measure the flow function (unconfined compression strength) of cohesive materials (mainly powders). In the UCT, the sample is first compressed (consolidated) under confined conditions, after which the same sample is compressed under unconfined conditions. If a tensile/compression machine is not available, dead loads can be used to apply the normal load incrementally. This is not ideal, but can provide enough information to estimate bulk stiffness. For further information see: Coetzee [11, 18], Lommen et al. [27], Thakur et al. [61], Donohue et al. [62].
Drop and pendulum tests 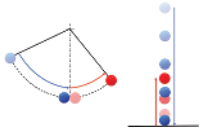	Scale invariant.	Particle–particle coefficient of restitution; particle–wall coefficient of restitution.	The tests are relatively easy and simple to execute, but a means to optically measure the particle motion is needed. Suitable for all particle sizes. Drop tests are not suitable for non-spherical particles, unless very sophisticated equipment and techniques are available to measure the 3D particle trajectory and spin.	Direct measurement of parameter values; hence, no need to replicate the test in a DEM simulation (DMA) For further information see: Barrios et al. [51], Yurata et al. [63], Hastie [64], Hlosta et al. [65], Elskamp et al. [37].

Penetration test 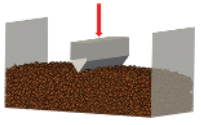	Scale variant due to the ratio of the tip to particle size.	Penetration resistance (resistance of the tip and shaft can be measured independently). If a transparent container is used, and the particles are coloured by layer, the flow field can be observed and measured.	The test apparatus is complex and requires an actuator to push the penetrometer into the material bed at a constant speed. The simulation is easier to set up. The tests are simple and quick to execute. Requires a large sample to cover the container. Suitable for all PSDs.	The container should be large enough to eliminate any wall boundary effects. For further information see: Mohajeri et al. [66, 67], Lommen et al. [42], Coetzee and Els [10].

1.7 Recommended Calibration Procedure for Non-cohesive and Slightly Cohesive Materials

As described earlier, the contact model parameters need to be determined by running a series of DEM simulations with varying parameters. The parameters can be varied systematically or through an optimisation algorithm. Ideally, in both approaches, an automated post-processing of the model results is required since a manual process would not be feasible for a large number of simulations.

The systematic variation of the parameter values over a whole range is time-consuming due to the high number of independent simulations required. However, this approach provides a deep understanding of the general relation between the simulated macroscopic (bulk) behaviour and the (individual) input parameters. Hence, this section focuses on the systematic approach, while Section 1.8 provides an overview of optimisation algorithms.

1.7.1 Ambiguous Parameter Combinations

The ideal situation would be to have an experiment of which the result is dependent on only a single parameter. If such an experiment is available for each of the unknown parameter values, calibration would be straightforward. Unfortunately, most numerical experiments are, however, sensitive to more than one parameter. As an example, take the very common AoR lifting cylinder test. Wensrich and Katterfeld [17] showed that (for non-cohesive materials) the AoR is dependent on both the particle–particle coefficient of sliding friction μ_{P} and the coefficient of rolling friction μ_{r}. When such results are plotted, a contour diagram results, which typically looks like the graph presented in Figure 1.3.

Figure 1.3 clearly demonstrates that there are an infinite number of parameter (μ_{P} and μ_{r}) combinations which result in the same value of the macroscopic AoR. This example highlights the problem of ambiguous parameter combinations. One calibration test result cannot provide a unique set of two (or more) contact model parameters. Hence, several test results are necessary to find a unique parameter set. The following section describes a procedure which solves the problem of ambiguous parameter combinations for non-cohesive materials.

This approach can also work for ‘slightly’ cohesive materials. However, with increasing bulk cohesive behaviour, the material flow increases in complexity and the test results are usually less consistent. Therefore, a larger number of tests are required to decrease the parameter range. To illustrate this point, a comparison of the AoR test with and without cohesion is shown in Figure 1.4. The calibration of cohesive materials is described in more detail in Section 1.7.

1.7.2 Solving for an Unambiguous Parameter Combination

The problem of ambiguous parameter combinations is equivalent to simultaneously solving a set of mathematical equations with a number of unknown variables or (calibration) parameters. A unique solution can only be obtained if the number of

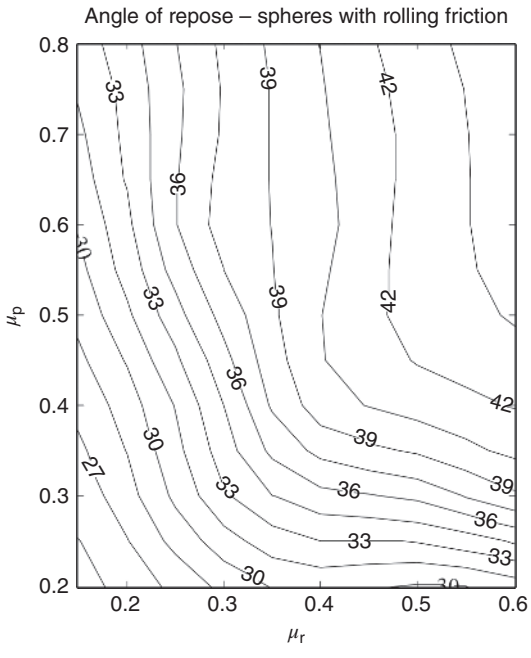

Figure 1.3 AoR simulation results according to Wensrich and Katterfeld et al. [17] using a lifting cylinder test for a systematic variation of particle–particle sliding friction μ_P and rolling friction μ_r. A constant macroscopic AoR is represented by an isoline. No cohesion was considered.

independent equations is equal to the number of variables. Using this analogy, the calibration test(s) should produce the same number (or more) of 'independent' test results as the number of DEM parameters to which the model is sensitive. The explanation in Section 1.4 and the summary in Table 1.1 help to identify the most influential parameter(s) for a given bulk property.

This analogy clearly explains why calibration tests which produce more than one test result (or bulk measure) are preferred. For example, the draw down test and the direct shear test produce four results each. However, not all of the test results can be called independent. For instance, the two AoR results and the remaining mass in the upper or lower chamber of the draw down test are dependent on each other. The higher the AoR in the upper chamber, the higher is the remaining mass in that chamber, and vice versa. In the direct shear test, the shear response at different normal stresses can be used as well as the internal friction angle and the time to reach failure.

For each bulk measure (either from a single test or multiple tests), a diagram such as the one presented in Figure 1.3 can be produced. The diagrams can then be superimposed to obtain a unique or unambiguous set of parameter values, i.e. a single set of parameter values which satisfies all test results. However, there is no guarantee that, in all cases, the isolines (one for each bulk measure) will intersect at a single point as described in Derakhshani et al. [36]. Often the measurement error needs to be considered to ensure a significant overlap of the test results as shown in detail by Roessler et al. [14].

Figure 1.5 shows how the different draw down test results (shear angle in the upper chamber, AoR in the lower chamber, mass in the lower chamber, and mass

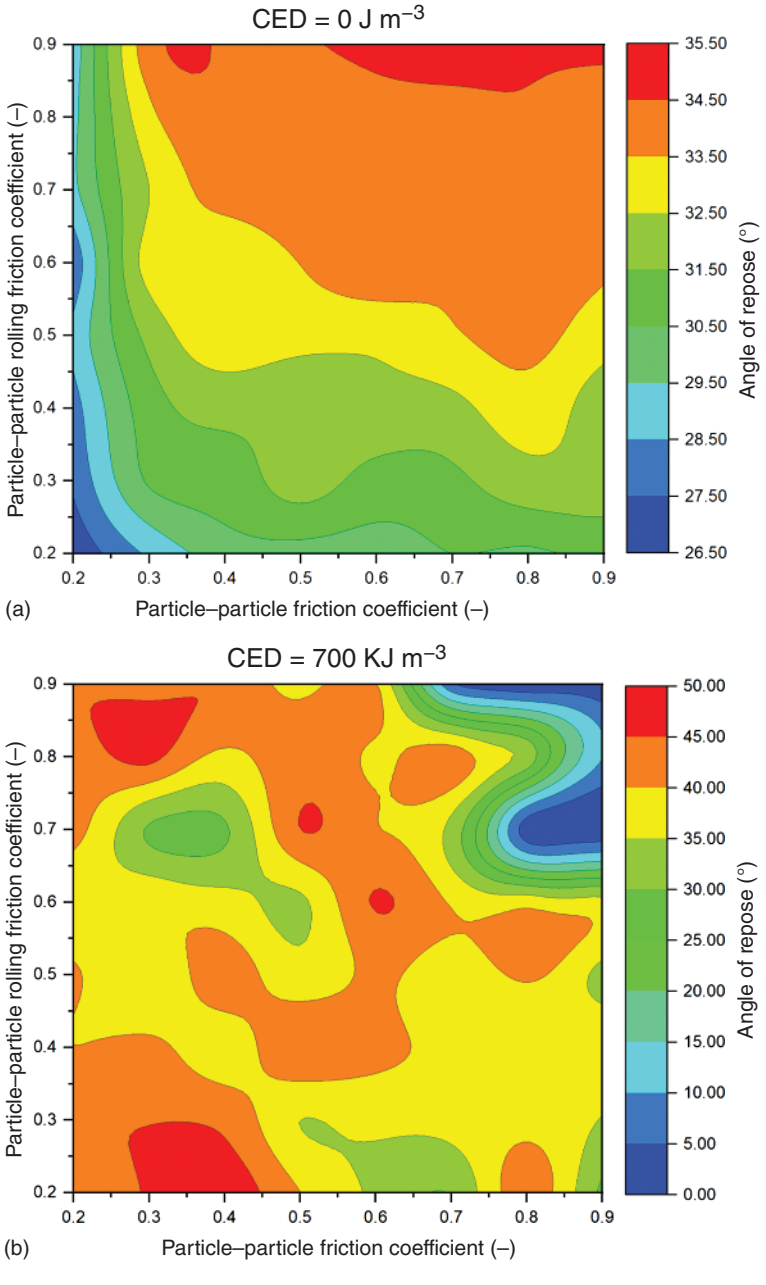

Figure 1.4 Comparison of AoR simulation results with varying particle–particle (sliding) friction and rolling friction coefficient for non-cohesive (a) and cohesive materials (b). Similar to Pachon-Morales et al. [43] for non-cohesive and slightly cohesive materials, a direct relation between the frictional values and the AoR can be shown. This is not the case for the cohesive material where a more irregular and complex behaviour can be seen.

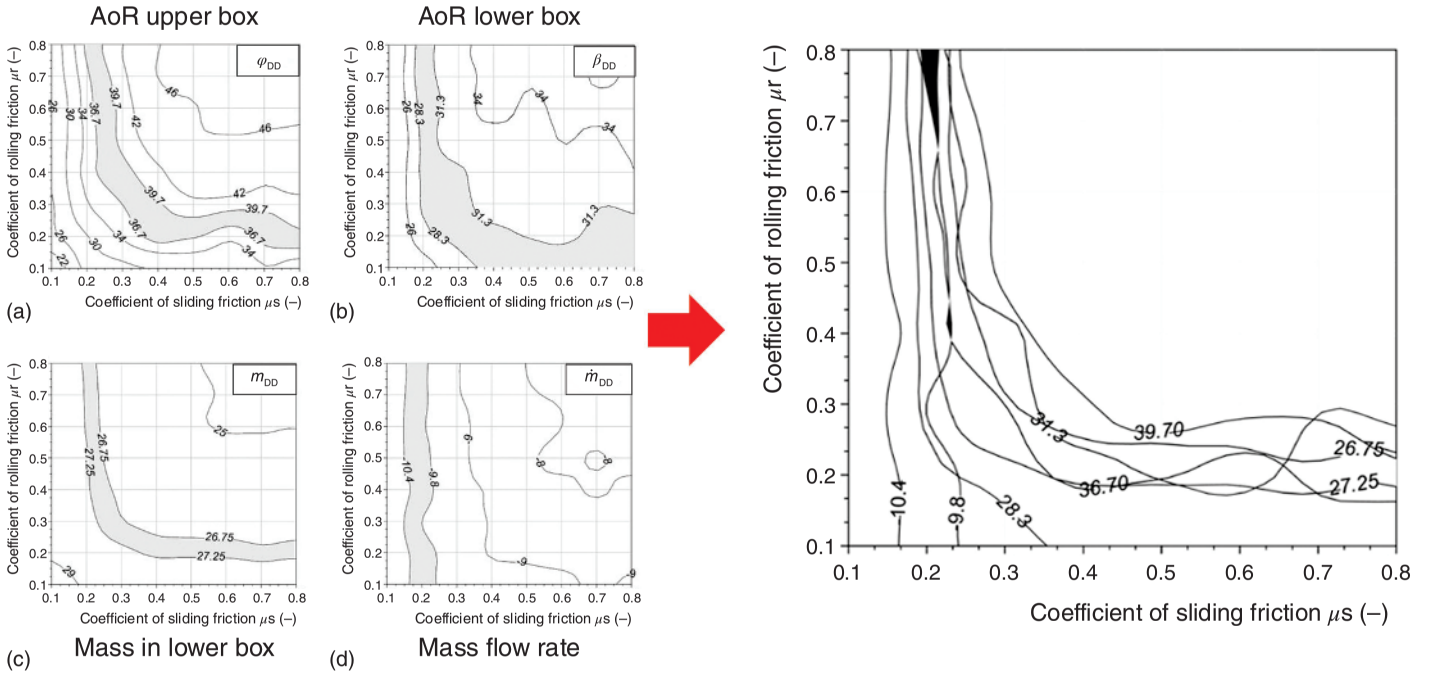

Figure 1.5 Combination of draw down test results for gravel with consideration of the measurement error for the identification of a unique parameter set. Source: Adapted from Roessler et al. [14].

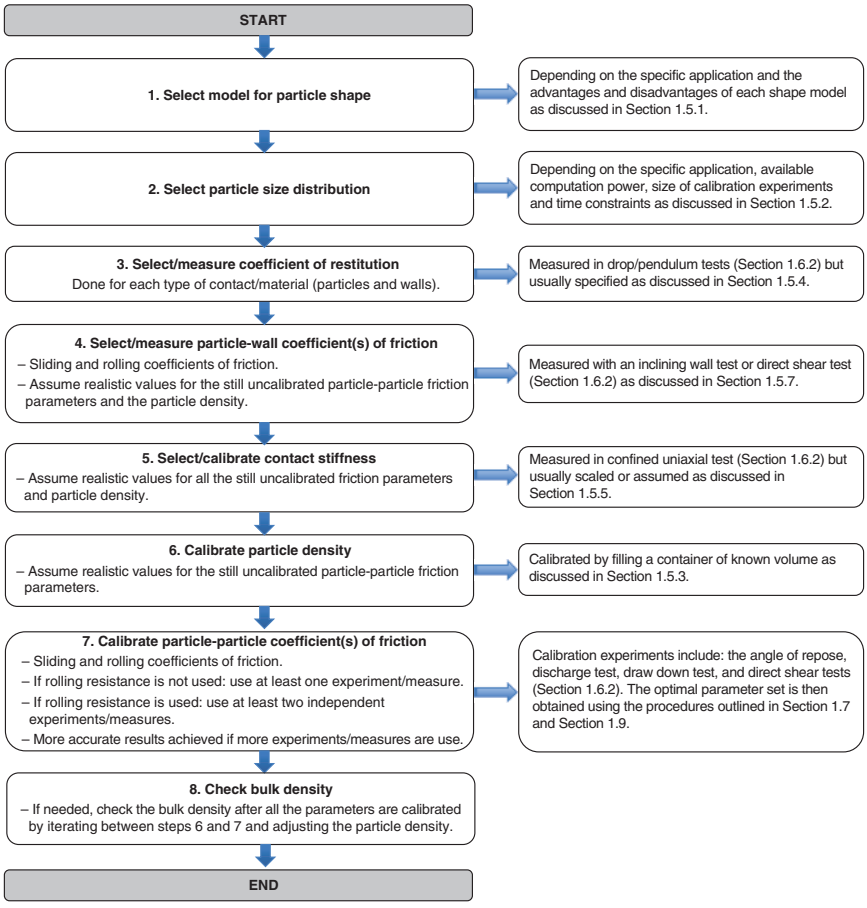

Figure 1.6 Calibration procedure for non-cohesive materials. Source: Adapted from Katterfeld et al. [28].

flow rate) can be plotted by taking the measurement error (grey marked areas in the diagrams on the left) into account. This significantly decreases the number of possible parameter combinations (sliding and rolling friction in this case) if the isolines of the contour plots are then overlaid as shown in the diagram on the right-hand side. The small black area in the right-hand side diagram shows the possible combination of the sliding and rolling friction which results in the same realistic shear angle, AoR, mass in the lower chamber, and the mass flow rate as measured in the experiment. Within the black area, the calculated cumulated error between simulated and measured test result allows the identification of a single parameter set.

The steps required to identify a unique set of DEM parameters can be summarised as follows:

1. Make use of a single calibration test with several independent bulk measures or a number of calibration tests, each with a single result or bulk measure. The latter case requires more effort in terms of experiments and simulations.

2. Determine the measurement errors for each test result (bulk measure) and consider them in the analysis of the DEM results.
3. Identify the parameter ranges which provide realistic simulation results for each test.
4. Calculate the cumulative error between simulation results and experimental measurements and identify the parameter set with a minimum error.

In the given examples of the lifting cylinder test (Figure 1.3) and the draw down test (Figure 1.5), only the influence of the particle–particle coefficients of sliding and rolling friction was shown. Although these two parameters are the ones which have the most significant influence on the modelled bulk behaviour of non-cohesive materials, the other parameters should also be carefully considered. This leads to the obvious question: is it necessary to vary all these parameter values systematically? This would require a tremendous number of independent simulation runs, which is not feasible. However, it has been shown that if the calibration procedure of individual parameters is executed in a specific sequence, the need for iterations and finding the unique (optimal) set of parameters can be minimised.

Based on the experience of a large number of academic and industrial experts, the calibration procedure as shown in the flowchart in Figure 1.6 was developed for non-cohesive materials, as presented in Katterfeld et al. [28]. The flowchart includes references to the sections where the influence of the specific parameter on the bulk behaviour is explained as well as the proposed experiment(s) to calibrate each parameter.

1.8 Outlook on the Calibration of Cohesive Materials

Cohesion, usually through the effects of moisture, can significantly alter the bulk behaviour of granular materials. However, the DEM research and modelling community do not yet have the same level of confidence in any DEM model to accurately predict the bulk behaviour of cohesive materials compared to that of non-cohesive materials. The exact reason for this is not known, and it might be that we are not yet able to successfully calibrate the cohesive parameters, and/or the cohesive contact models that are currently available do not capture the real physics accurately enough. For completeness, a short summary of the published attempts made to calibrate cohesive materials is presented here.

Grima [68] and Grima and Wypych [49] developed and validated a strategy for calibrating the parameters of dry and wet black coal and bauxite. First, the material was calibrated in a dry non-cohesive state based on flow property measurements and bench scale tests and using the Hertz–Mindlin (no slip) contact model. Thereafter, the material was tested in a moist cohesive state and the appropriate cohesive parameters introduced to the DEM contact model. The cohesive parameters were calibrated, while the non-cohesive parameter values remained unchanged. Two experimental tests were used to calibrate the parameters. First, a swing-arm slump test with a split cylinder was developed to measure the AoR. The second test was

based on a cylindrical draw down test, where the shear angle (upper box), poured AoR (lower box), and the mass flow rate (estimated from high-speed photography) were measured. In addition, the impact force of the material onto the bottom plate was measured.

Due to the cohesive effects, the shape of the formed piles was irregular, which made it difficult to define the AoR in the slump test. A quantitative approach was then followed, and the general shape of the heap used for comparison. In the draw down test, the cohesive material slumped down onto the lower plate, and the cohesive parameter (the cohesive energy density) had no significant effect on the poured AoR. However, it had a significant effect on the shear angle, and in the end, this was the only measured parameter from the draw down test that could be used for calibration purposes. However, a single value of the cohesion energy density, which accurately predicted the slump test AoR and the draw down shear angle, could not be found. In the end, the study concluded that a calibrated cohesion parameter for one system might not be suitable for another system.

Katterfeld et al. [69] used two different cohesive contact models and the draw down test to calibrate the parameters for wet gypsum. Both models under-predicted the shear angle in the upper box of the draw down test and over-predicted the poured AoR in the lower box.

Roessler and Katterfeld [29] made use of the lifting cylinder test to calibrate the cohesive parameter for wet sand. The AoR showed a very high level of variability, ranging from 40.4° to 84.3° for the same material in repeated tests. Hence, the macroscopic flow behaviour was rather analysed where three distinct and reproducible phases could be identified during the upward motion of the cylinder and used as calibration criteria. This study, however, made use of a single moisture content, and this approach still needs to be verified for different moisture contents and different bulk materials.

Ajmal et al. [70], on the other hand, showed that the draw down test could be used to successfully calibrate sliding friction, rolling friction, and cohesion parameter for wet sand (10% moisture content). It was shown that the blockage or arching of material at the opening was independent of sliding and rolling friction and depended only on the cohesion parameter. Comparing these results to experimental observations for various opening sizes, a narrow band of values for the cohesion parameter could be established. A unique set of parameter values could then be obtained by comparing the AoR, formed in the lower box, and the total mass that flowed to the bottom box, to experimental measurement. It was noted that the shear angle, formed in the upper box, could not be used since it was not reproducible.

Mohajeri et al. [57] used the ring shear test to calibrate the parameters of cohesive (moist) coal by using an elasto-plastic cohesion contact model. This work was further extended [71] in a study where a combination of calibration experiments was used to calibrate the parameters of cohesive iron ore. The tests included a ring shear test, a shear box (ledge AoR), and a penetration test.

Carr et al. [72] investigated the use of two contact models to simulate the behaviour of cohesive iron ore with varying moisture content. The material was allowed to flow from a feeding conveyor onto an impact plate, where the build-up of material was observed. It was concluded that only the liquid-bridge model was capable of

simulating the clumping effect of the material which was observed during the experiments. In a further study [73], a combination of the shear box (ledge test), draw down, and a conveyor impact plate test was used. By varying the cohesive parameter, the draw down test was used to investigate flowing and arching cases. The irregular slopes that formed made it difficult to measure the angles, and it was concluded that in the shear box and the draw down test, the residual mass was a more definite and reproducible calibration measure.

1.9 Optimisation Approaches Applied to the Calibration Process

An increasing number of calibration parameters increases the problem of ambiguous parameter sets and brings classical visualisation techniques such as the contour plots, shown in Section 1.6, to their limits. Hence, if more than two parameters should be calibrated, for example, if one would include cohesion or particle upscaling, the use of optimisation algorithms might be mandatory. Also, an increasing number of calibration test results such as an AoR, shear angle, and mass flow rate from a draw down test or different yield loci from a direct shear test lead to complex analyses with a lot of processing steps. The aim of the calibration process is to find a set of DEM parameter values in such a way that the simulation results of the physical calibration experiments are the most accurate (optimal) as compared to the experimental results. Hence, the task of the optimisation process is to minimise the difference between the experimental and simulation results.

It was already discussed that multiple calibration test results are necessary for finding an unambiguous parameter set. The calibration test results are the so-called objective function values or target values for the optimisation algorithm. Hence, only such algorithms can be used which can handle multiple target values. However, besides the problem of handling multiple parameters and multiple target criteria, the biggest advantage of optimisation algorithms is the reduced number of calibration simulations. This addresses one of the largest bottlenecks in the whole calibration process, namely the time required to run a whole series of calibration simulations.

Different optimisation schemes are available, and Richter et al. [74] identified the following characteristics of typical DEM results as significant to consider in the selection process:

- nonlinear objective function topology,
- expensive computation,
- gradients cannot be obtained directly,
- limitations of the search space in the form of parameter boundaries (restricted optimization problem),
- there can be more than one optimum or many local optima,
- rough objective function surface due to stochastic effects and numerical noise,
- more than one objective function value is necessary for calibration,
- discontinuities can occur (e.g. bridging in funnel flow experiments due to high friction values).

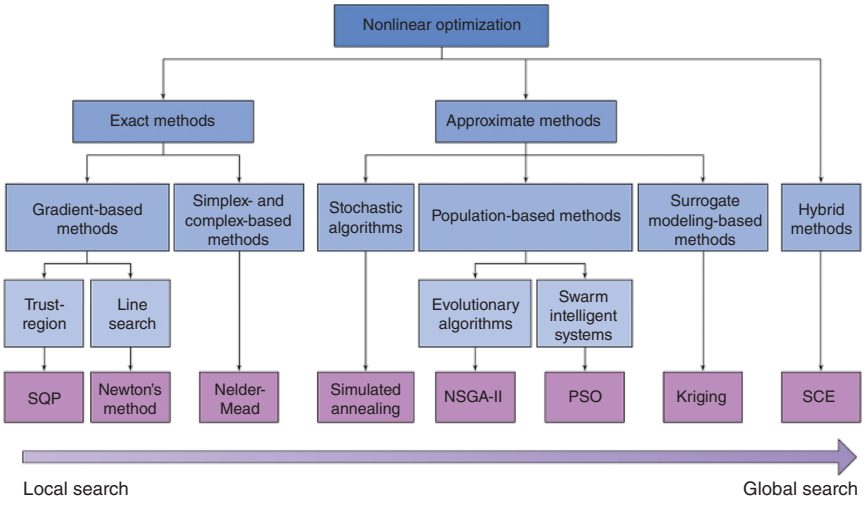

Figure 1.7 Overview of optimisation algorithm. SQP = sequential quadratic programming, NSGA = non-dominated sorting genetic algorithm, PSO = particle swarm optimization, SCE = shuffled complex evolution. Source: Richter et al. [74]/with permission of Elsevier.

Richter et al. [74] also provides a comprehensive overview of the different optimisation approaches which are generally known (Figure 1.7). A systematic review of these approaches is essential since different terms are used in literature for the same optimisation approach. For example, Hess et al. [75] used the term particle swarm optimisation whereas Do et al. [35] used the term genetic algorithms.

An increasing number of publications explain the use of 'Artificial Intelligence' or 'Machine Learning' to optimise the calibration process. However, often the actual algorithm used is similar to those from publications which make use of different terms.

For the DEM application, the use of surrogate models can be identified as one of the best optimisation approaches. Many DEM publications focus on this approach. Most surrogate models are capable of identifying a global optimum on a rough objective function surface with many local optima within a few iterations. Further, they can consider parameter limitations and multi-objective problems and discontinuities.

The surrogate model approach generates, in the first step, a virtual approximation of the objective functions. Only a few calibration simulations are necessary for this. The sampling method for selecting the initial parameters is an important step. Based on the generated surrogate model, a set of optimised parameters is predicted and evaluated by the so-called acquisition function. Then, an additional calibration simulation is undertaken, and the difference to the target values is calculated. If the difference is larger than stopping criteria, the surrogate model is refined by the new simulation results and the whole process is repeated. Richter et al. [74] have suggested a general description of the necessary steps to use the surrogate model approach. The flow diagram in Figure 1.8 summarises the flow of the so-called Generalised Surrogate Modelling-based Calibration (GSMC).

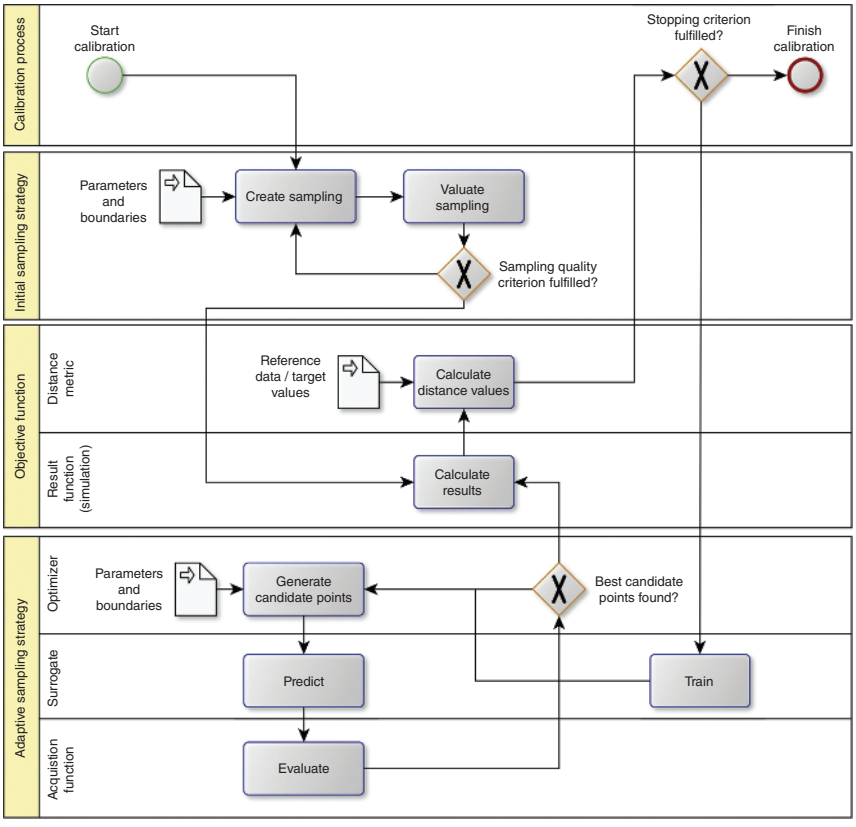

Figure 1.8 Component structure and process of generalised surrogate modelling-based calibration (GSMC). Source: Richter et al. [74]/with permission of Elsevier.

To calculate and predict the surrogate model, several approaches are known. They can be separated in probabilistic and non-probabilistic approaches. Probabilistic surrogate models include the calculation of the probability for the prediction of the estimated value, which provides advantages in the evaluation process. Richter et al. [74] have analysed a number of different surrogate algorithms, which include Gaussian process regression (GPR), artificial neural networks, multi-adaptive regression splines, and universal Kriging. Rackl and Hanley [76] and Kriging and Benvenuti et al. [77] used artificial neural networks. Richter et al. [74] could achieve the best results with the GPR which belongs to the probabilistic approaches. Due to the probabilistic surrogate model and the probabilistic acquisition function, the approach can be classified as a Bayesian optimisation approach. This approach and the Gaussian model were also used by Hartmann et al. [78].

Since Richter et al. [74] and Roessler et al. [14] used the same calibration tests and data, it could be shown that the use of the optimisation algorithm resulted in the same final DEM parameter set as the systematic parameter selection process where a full factorial design was used. While the systematic selection process required at least 64 simulation runs, the GSMC with GPR needed less than 23 simulation runs.

1.10 Conclusion

This chapter discusses one of the most important requirements for the successful application of the DEM: an understanding of how the DEM parameters influence the bulk behaviour of granular materials, and why a calibration of these parameters is absolutely necessary if accurate simulation results are to be achieved. The most important parameters used in almost all DEM models were presented, and their general influence on simulated results was discussed.

The most commonly used calibration tests were described as well as the problem of ambiguous parameter sets, which require calibration tests with several measurable outcomes (bulk measures). A standard process for the calibration of non- and slightly cohesive materials was presented, and it was discussed why the calibration of cohesive materials is much more problematic and still a matter of research.

Finally, the use of optimisation algorithms for an efficient calibration process was described. Such algorithms might be an essential prerequisite for the complex task of calibrating cohesive materials.

Although the calibration process is essential for the successful application of DEM, no available DEM software addresses this issue with a predefined workflow, including both pre- and postprocessing. Most DEM software have a batch feature to run a series of simulations with automated parameter variation. For the automated calibration using optimisation algorithms, open source software packages such as Decalioc or GrainLearning exist, but they demand a deep understanding of the whole procedure and require programming skills.

This is one reason why the calibration of DEM parameters – although very necessary and important – is often performed by experts in the field as a consulting service. Such services must include suitable experimental tests and the run and analysis of a series of calibration simulations. Experience proves that, with the current state of the art in DEM calibration, knowledge of the physical behaviour of bulk materials in close combination with simulation know-how is required to obtain accurate calibration results. However, metamodel-based approaches like those described by Richter and Will [79] might lead to an improved understanding of the DEM parameters and their influence on the macroscopic behaviour of bulk materials and, in the future, significantly reduce the complexity of the calibration process.

Glossary

Angle of repose
Bulk calibration approach
Bulk cohesion
Bulk density
Bulk friction
Bulk stiffness
Calibration philosophies
Calibration process
Calibration test

Coarse graining
Coefficient of restitution
Cohesive material
Combined scaling
Contact damping
Contact model
Contact properties
Contact stiffness
DEM parameters
Direct measurement approach
Dissipation of energy
Draw down test
Exact scaling
Hybrid scaling
Lifting cylinder
Multi-sphere particle
Non-cohesive material
Optimisation
Parameter combination
Parameter set
Particle density
Particle shape
Particle size distribution
Physical bulk properties
Porosity
Rolling friction
Scalping
Sliding friction

References

1 Coetzee, C.J., Basson, A.H., and Vermeer, P.A. (2007). Discrete and continuum modelling of excavator bucket filling. *Journal of Terramechanics* 44: 177–186.
2 Cundall, P.A. and Strack, O.D. (1979). Discrete numerical model for granular assemblies. *Géotechnique* 29 (1): 47–65.
3 O'Sullivan, C. (2011). *Particulate discrete element modelling, a geomechanics perspective, Applied Geotechnics*, vol. 4. London and New York: Spon Press ISBN13: 978-0-203-88098-2.
4 Thornton, C. (2015). *Granular dynamics, contact mechanics and particle system simulation, A DEM study*. Cham: Springer ISBN 978-3-319-18710-5.
5 Hazzar, L., Nuth, M., and Chekired, M. (2020). DEM simulation of drained triaxial tests for glass-beads. *Powder Technology* 364: 123–134.
6 Mesnier, A., Peczalski, R., Mollon, G., and Vessot-Crastes, S. (2020). Mixing of bi-dispersed milli-beads in a rotary drum: mechanical segregation analyzed by lab-scale experiments and DEM simulation. *Processes* 8 (9): 1166.

7 Coetzee, C.J. (2017). Review: calibration of the discrete element method. *Powder Technology* 310: 104–142.

8 Mitarai, N. and Nori, F. (2006). Wet granular materials. *Advances in Physics* 55 (1, 2): 1–45.

9 Seville, J.P.K., Willet, C.D., and Knight, P.C. (2000). Interparticle forces in fluidisation: a review. *Powder Technology* 113: 261–268.

10 Coetzee, C.J. and Els, D.N.J. (2009). Calibration of discrete element parameters and the modelling of silo discharge and bucket filling. *Computers and Electronics in Agriculture* 65: 198–212.

11 Coetzee, C.J. (2020). Calibration of the discrete element method: strategies for spherical and non-spherical particles. *Powder Technology* 364: 851–878.

12 Guo, Y., Zhao, C., Markine, V. et al. (2020). Discrete element modelling of railway ballast performance considering particle shape and rolling resistance. *Railway Engineering Science* 28: 382–407.

13 Markauskas, D., Ramírez-Gómez, A., Kacianauskas, R., and Zdancevicius, E. (2015). Maize grain shape approaches for DEM modelling. *Computers and Electronics in Agriculture* 118: 247–258.

14 Roessler, T., Richter, C., and Katterfeld, A. (2019b). Development of a standard calibration procedure for the DEM parameters of cohesionless bulk materials. Part I - solving the problem of ambiguous parameter combinations. *Powder Technology* 343: 803–812.

15 Wensrich, C.M., Katterfeld, A., and Sugo, D. (2014). Characterisation of the effects of particle shape using a normalised contact eccentricity. *Granular Matter* 16 (3): 327–337.

16 Ai, J., Chen, J.F., Rotter, J.M., and Ooi, J.Y. (2011). Assessment of rolling resistance models in discrete element simulations. *Powder Technology* 206: 269–282.

17 Wensrich, C. and Katterfeld, A. (2012). Rolling friction as a technique for modelling particle shape in DEM. *Powder Technology* 217: 409–417.

18 Coetzee, C.J. (2016). Calibration of the discrete element method and the effect of particle shape. *Powder Technology* 297: 50–70.

19 Stahl, M. and Konietzky, H. (2011). Discrete element simulation of ballast and gravel under special consideration of grain-shape, grain-size and relative density. *Granular Matter* 13: 417–428.

20 Chen, W., Donohue, T., Katterfeld, A., and Williams, K. (2017). Comparative discrete element modelling of a vibratory sieving process with spherical and rounded polyhedron particles. *Granular Matter* 19 (81) 1–12.

21 Alonso-Marroquín, F., Ramírez-Gómez, A., González-Montellano, C. et al. (2013). Experimental and numerical determination of mechanical properties of polygonal wood particles and their flow analysis in silos. *Granular Matter* 15: 811–826.

22 Lenaerts, B., Aertsen, T., Tijskens, E. et al. (2014). Simulation of grain–straw separation by discrete element modeling with bendable straw particles. *Computers and Electronics in Agriculture* 101: 24–33.

23 Thakur, S.C., Ooi, J.Y., and Ahmadian, H. (2016). Scaling of discrete element model parameters for cohesionless and cohesive solid. *Powder Technology* 293: 130–137.

24 Roessler, T. and Katterfeld, A. (2018). Scaling of the angle of repose test and its influence on the calibration of DEM parameters using upscaled particles. *Powder Technology* 330: 58–66.

25 Mohajeri, M.J., Helmons, R.L., van Rhee, C., and Schott, D.L. (2020a). A hybrid particle-geometric scaling approach for elasto-plastic adhesive DEM contact models. *Powder Technology* 369: 72–87.

26 Katterfeld, A., Donohue, T., and Ilic, D. (2012). Application of the discrete element method in mechanical conveying of bulk materials. In: *07th International Conference for Conveying and Handling of Particulate Solids*, 10–13 September 2012, Friedrichshafen, Germany.

27 Lommen, S., Schott, D.L., and Lodewijks, G. (2014). DEM speedup: stiffness effects on behaviour of bulk material. *Particuology* 12: 107–112.

28 Katterfeld, A., Coetzee, C., Donohue, T., et al. (2019). White Paper: Calibration of DEM parameters for cohesionless bulk materials under rapid flow conditions and low consolidation. https://www.researchgate.net/publication/334129169_Calibration_of_DEM_Parameters_for_Cohesionless_Bulk_Materials_under_Rapid_Flow_Conditions_and_Low_Consolidation.

29 Roessler, T. and Katterfeld, A. (2019a). DEM parameter calibration of cohesive bulk materials using a simple angle of repose test. *Particuology* 45: 105–115.

30 Tan, Y., Yu, Y., Fottner, J., and Kessler, S. (2021). Automated measurement of the numerical angle of repose (aMAoR) of biomass particles in EDEM with a novel algorithm. *Powder Technology* 388: 462–473.

31 Muller, D., Fimbinger, E., and Brand, C. (2021). Algorithm for the determination of the angle of repose in bulk material analysis. *Powder Technology* 373: 598–605.

32 Klanfar, M., Korman, T., Domitrovic, D., and Herceg, V. (2021). Testing the novel method for angle of repose measurement based on area-weighted average slope of a triangular mesh. *Powder Technology* 387: 396–405.

33 Qi, L., Chen, Y., and Sadek, M. (2019). Simulations of soil flow properties using the discrete element method (DEM). *Computers and Electronics in Agriculture* 157: 254–260.

34 Zhou, L., Yu, J., Liang, L. et al. (2021). DEM parameter calibration of maize seeds and the effect of rolling friction. *Processes* 9 (914): https://doi.org/10.3390/pr9060914.

35 Do, H.Q., Aragon, A.M., and Schott, D.L. (2018). A calibration framework for discrete element model parameters using genetic algorithms. *Advanced Powder Technology* 29: 1393–1403.

36 Derakhshani, S.M., Schott, D.L., and Lodewijks, G. (2015). Micro macro properties of quartz sand: experimental investigation and DEM simulation. *Powder Technology* 269: 127–138.

37 Elskamp, F., Kruggel-Emden, H., Henning, M., and Teipel, U. (2017). A strategy to determine DEM parameters for spherical and non-spherical particles. *Granular Matter* 19 (46): 1–13.

38 Horabik, J., Parafinuik, P., and Molenda, M. (2017). Discrete element modelling study of force distribution in a 3D pile of spherical particles. *Powder Technology* 312: 194–203.

39 Wang, L., Li, R., Wu, B. et al. (2018). Determination of the coefficient of rolling friction of an irregularly shaped maize particle group using physical experiment and simulations. *Particuology* 38: 185–195.

40 Fu, J.-J., Chen, C., Ferellec, J.-F., and Yang, J. (2020). Effect of particle shape on repose angle based on hopper flow test and discrete element method. *Advances in Civil Engineering* 2020: 8811063. https://doi.org/10.1155/2020/8811063.

41 Chen, Z., Wassgren, C., Veikle, E., and Ambrose, K. (2020). Determination of material and interaction properties of maize and wheat kernels for DEM simulation. *Biosystems Engineering* 195: 208–226.

42 Lommen, S., Mohajeri, M., Lodewijks, G., and Schott, D. (2019). DEM particle upscaling for large-scale bulk handling equipment and material interaction. *Powder Technology* 352: 273–282.

43 Pachon-Morales, J., Do, H., Colin, J. et al. (2019). DEM modelling for flow of cohesive lignocellulosic biomass powders: model calibration using bulk tests. *Advanced Powder Technology* 30: 732–450.

44 Coetzee, C.J. (2019). Particle upscaling: calibration and validation of the discrete element method. *Powder Technology* 344: 487–503.

45 Rong, W., Feng, Y., Schwartz, P. et al. (2020). Sensitivity analysis of particle contact parameters for DEM simulation in a rotating drum using response surface methodology. *Powder Technology* 362: 604–614.

46 Balevicius, R., Kacianauskas, R., Mroz, Z., and Sielamowicz, I. (2006). Discrete element method applied to multiobjective optimization of discharge flow parameters in hoppers. *Structural and Multidisciplinary Optimization* 31: 163–175.

47 Hlosta, J., Jezerská, L., Rozbroj, J. et al. (2020). DEM investigation of the influence of particulate properties and operating conditions on the mixing process in rotary drums: part 1 – determination of the DEM parameters and calibration process. *Processes* 8 (222): https://doi.org/10.3390/pr8020222.

48 Coetzee, C. and Nel, R. (2014). Calibration of discrete element properties and the modelling of packed rock beds. *Powder Technology* 264: 332–342.

49 Grima, A.P. and Wypych, P.W. (2011). Development and validation of calibration methods for discrete element modelling. *Granular Matter* 13: 127–132.

50 Zhou, Y.C., Xu, B.H., Yu, A.B., and Zulli, P. (2002). An experimental and numerical study of the angle of repose of coarse spheres. *Powder Technology* 125: 45–54.

51 Barrios, G.K.P., de Carvalho, R.M., Kwade, A., and Tavares, L.M. (2013). Contact parameter estimation for DEM simulation of iron ore pellet handling Gabriel. *Powder Technology* 248: 84–93.

52 Agarwal, A., Tripathi, A., Tripathi, A. et al. (2021). Rolling friction measurement of slightly non-spherical particles using direct experiments and image analysis. *Granular Matter* 23 (60): 1–14.

53 ASTM D3080/D3080M (2011). *Standard test method for direct shear test of soils under consolidated drained conditions*. West Conshohocken, PA: ASTM International.

54 ISO 17892-10:2018(2018). Geotechnical investigation and testing — Laboratory testing of soil — Part 10: Direct shear tests.

55 ASTM D6773-16 (2016). *Standard test method for bulk solids using schulze ring shear tester*.

56 Simons, T.A.H., Weiler, R., Strege, S. et al. (2015). A ring shear tester as calibration experiment for DEM simulations in agitated mixers – a sensitivity study. *Procedia Engineering* 102: 741–748.

57 Mohajeri, M.J., Do, H.Q., and Schott, D.L. (2020b). DEM calibration of cohesive material in the ring shear test by applying a genetic algorithm framework. *Advanced Powder Technology* 31 (5): 1838–1850.

58 Bian, X., Li, W., Qian, Y., and Tutumluer, E. (2019). Micromechanical particle interactions in railway ballast through DEM simulations of direct shear tests. *International Journal of Geomechanics* 19 (5): 1–19.

59 Falke, T., de Payrebrune, K.M., Kirchhof, S. et al. (2018). An alternative DEM parameter identification procedure based on experimental investigation: a case study of a ring shear cell. *Powder Technology* 328: 227–234.

60 Grima, A. and Wypych, P. (2013). Effect of particle properties on the discrete element simulation of wall friction. In: *ICBMH 2013 - 11th International Conference on Bulk Materials Storage, Handling and Transportation*.

61 Thakur, S.C., Ahmadian, H., Sun, J., and Ooi, J.Y. (2014). An experimental and numerical study of packing, compression, and caking behaviour of detergent powders. *Particuology* 12: 2–12.

62 Donohue, T.J., Wensrich, C.M., and Reid, S. (2016). On the use of the uniaxial shear test for DEM calibration. In: *The 7th International Conference on Discrete Element Methods*. China: Dalian (1–4 August 2016).

63 Yurata, T., Gidaspow, D., Piumsomboon, P., and Chalermsinsuwan, B. (2021). The importance of parameter-dependent coefficient of restitution in discrete element method simulations. *Advanced Powder Technology* 32: 1004–1012.

64 Hastie, D.B. (2013). Experimental measurement of the coefficient of restitution of irregular shaped particles impacting on horizontal surfaces. *Chemical Engineering Science* 101: 828–836.

65 Hlosta, J., Zurovec, D., Rozbroj, J. et al. (2018). Experimental determination of particle–particle restitution coefficient via double pendulum method. *Chemical Engineering Research and Design* 135: 222–233.

66 Mohajeri, M., van Rhee, C., and Schott, D.L. (2018). Penetration resistance of cohesive iron ore: a DEM study. In: *9th International Conference on Conveying and Handling of Particulate Solids, CHoPS 2018*.

67 Mohajeri, M.J., de Kluijver, W., Helmons, R.L.J. et al. (2021a). A validated co-simulation of grab and moist iron ore cargo: replicating the cohesive and stress-history dependent behaviour of bulk solids. *Advanced Powder Technology* 32 (4): 1157–1169.

68 Grima, A.P. (2011). Quantifying and modelling mechanisms of flow in cohesionless and cohesive granular materials. PhD thesis. University of Wollongong.

69 Katterfeld, A., Roessler, T., and Chen, W. (2018). Calibration of the DEM parameters of cohesive bulk materials for the optimisation of transfer chutes. In: *CHoPS 2018, 9th International Conference on Conveying and Handling of Particulate Solids*. (10th–14th September 2018).

70 Ajmal, M., Roessler, T., Richter, C., and Katterfeld, A. (2020). Calibration of cohesive DEM parameters under rapid flow conditions and low consolidation stresses. *Powder Technology* 374: 22–32.

71 Mohajeri, M.J., van Rhee, C., and Schott, D.L. (2021b). Replicating cohesive and stress-history-dependent behavior of bulk solids: feasibility and definiteness in DEM calibration procedure. *Advanced Powder Technology* 32: 1532–1548.

72 Carr, M.J., Chen, W., Williams, K., and Katterfeld, A. (2016). Comparative investigation on modelling wet and sticky material behaviours with a simplified JKR cohesion model and liquid bridging cohesion model in DEM. In: *ICBMH 2016 - 12th International Conference on Bulk Materials Storage, Handling and Transportation, Proceedings*.

73 Carr, M.J., Roessler, T., Otto, H. et al. (2019). Calibration procedure of discrete element method (DEM) parameters for cohesive bulk materials. In: *13th International Conference on Bulk Materials Storage, Handling & Transportation*.

74 Richter, C., Roessler, T., Kunze, G. et al. (2019). Development of a standard calibration procedure for the DEM parameters of cohesionless bulk materials – part II: efficient optimization-based calibration. *Powder Technology* 360: 967–976. https://doi.org/10.1016/j.powtec.2019.10.052.

75 Hess, G., Richter, C., and Katterfeld, A. (2016). Simulation of the dynamic interaction between bulk material and heavy equipment - calibration and validation. In: *ICBMH 2016: 12th International Conference on Bulk Materials Storage, Handling and Transportation; Proceedings, 11–14 July 2016* (ed. D. Hastie), 427–436. Darwin, Australia: The Institution of Engineers.

76 Rackl, M. and Hanley, K.J. (2016). A methodical calibration procedure for discrete element models. *Powder Technology* 307: 73–83. https://doi.org/10.1016/j.powtec.2016.11.048.

77 Benvenuti, L., Kloss, C., and Pirker, S. (2016). Identification of DEM simulation parameters by Artificial Neural Networks and bulk experiments. *Powder Technology* 291: 456–465. https://doi.org/10.1016/j.powtec.2016.01.003.

78 Hartmann, P., Cheng, H., and Thoeni, K. (2021). Performance study of iterative Bayesian filtering to develop an efficient calibration framework for DEM. *Computers and Geotechnics* 141: https://doi.org/10.1016/j.compgeo.2021.104491.

79 Richter, C. and Will, F. (2021). Introducing metamodel-based global calibration of material-specific simulation parameters for discrete element method. *Minerals* 11: 848. https://doi.org/10.3390/min11080848.